MAX-PLANCK-GESELLSCHAFT

Journal of Catalysis 291 (2012) 44-54

AC FHI

Catalytic reactivity of face centered cubic $PdZn_{\alpha}$ for the steam reforming of methanol

B. Halevi[1,*], E. J. Peterson[1], A. Roy[1], A. DeLariva[1], E. Jeroro[2], F. Gao[3], Y. Wang[3,4], J. M. Vohs[2], B. Kiefer[5], E. Kunkes[6], M. Havecker[6], M. Behrens[6], R. Schlögl[6], A. K. Datye[1,*]

[1]Department of Chemical & Nuclear Engineering and Center for Microengineered Materials, MSC01 1120, University of New Mexico, Albuquerque, NM 87131-0001, USA.
[2]Department of Chemical and Biomolecular Engineering, University of Pennsylvania, Philadelphia, Pennsylvania 19104.
[3]The Gene & Linda Voiland School of Chemical Engineering and Bioengineering, Washington State University, Pullman WA 99164-2710 (USA)
[4]Institute for Integrated Catalysis, Pacific Northwest National Laboratory, Richland, WA 99352, USA
[5]Department of Physics, New Mexico State University, Las Cruces, NM, 88003
[6]Department of Inorganic Chemistry, Fritz-Haber-Institute of the Max-Planck-Society, Faradayweg 4–6, D-14195 Berlin, Germany

[*] Corresponding author: e-mail datye@unm.edu, halevi@unm.edu

Received 24 October 2011; Article available online: 17 May 2012; Published July 2012

Abstract

Addition of Zn to Pd changes its catalytic behavior for steam reforming of methanol. Previous work shows that improved catalytic behavior (high selectivity to CO_2) is achieved by the intermetallic, tetragonal $L1_0$ phase $PdZn_{b1}$, where the Pd:Zn ratio is near 1:1. The Pd-Zn phase diagram shows a number of other phases, but their steady state reactivity has not been determined due to the difficulty of precisely controlling composition and phase in supported catalysts. Hence, the role of Zn on Pd has generally been studied only on model single crystals where Zn was deposited on Pd(111) with techniques such as TPD and TPR of methanol or CO. The role of small amounts of Zn on the steady state reactivity of Pd-Zn remains unknown. Therefore, in this work, we have synthesized unsupported powders of phase pure $PdZn_a$, a solid solution of Zn in fcc Pd, using a spray-pyrolysis technique. The surface composition and chemical state were studied using Ambient Pressure XPS (AP-XPS) and were found to match the bulk composition and remain so during methanol steam reforming (MSR) (P_{tot} = 0.25 mbar). Unlike the $PdZn_{b11}$ phase, we find that $PdZn_a$ is 100% selective to CO during methanol steam reforming with TOF at 250°C of 0.12 s^{-1}. Steady state ambient pressure microreactor experiments and vacuum TPD of methanol and CO show that the a phase behaves much like Pd, but Zn addition to Pd improves TOF since it weakens the Pd-CO bond, eliminating the poisoning of Pd by CO during MSR over Pd. The measured selectivity for fcc $PdZn_a$ therefore confirms that adding small amounts of Zn to Pd is not enough to modify the selectivity during MSR, and that the $PdZn_{b1}$ tetragonal structure is essential for CO_2 formation during MSR.

Keywords: PdZn; Methanol steam reforming, MSR; Heterogeneous catalysis

1. Introduction

The objective of this study was to investigate the role of phase and composition of Pd-Zn for the steam reforming of methanol. As the concentration of Zn in Pd is increased, the phase diagram shows regions of immiscibility as well as a number of stable phases[1]. The reactivity of each of these phases, and the role of composition within each phase, cannot be studied with conventional supported catalysts, such as Pd/ZnO, due to the inherent heterogeneity of composition and phase among individual nanoparticles. We have previously demonstrated that aerosol synthesis yields metal powders with a high degree of uniformity in composition and phase[2]. The surface area of these aerosol derived metal powders is high enough to perform measurements of their catalytic behavior as well as surface properties[3]. In this work, we use this approach of aerosol synthesis to prepare samples of fcc Pd wherein the Zn is

incorporated to form a solid solution, the so-called alpha phase in the PdZn phase diagram. This helps answer the question of whether the intermetallic PdZn phase is necessary for achieving high CO_2 selectivity during steam reforming of methanol, or whether smaller amounts of Zn incorporated within fcc Pd are sufficient for changing the selectivity of Pd.

Pd/ZnO has been shown to have excellent selectivity and stability for Methanol Steam Reforming.[4] It has been proposed that the reaction of methanol to CO_2 proceeds via hydration of a methyl formate intermediate[5], and the active phase was suggested to be the PdZn intermetallic having a $L1_0$ structure that can be formed through Pd/ZnO reduction.[6] Subsequent studies attempted to better understand and quantify the activity, including confirmation of the reaction intermediates, the pathway, and active phase on both model single crystal and supported samples.[7-11] One of the drawbacks to the Pd/ZnO system is the rapid sintering of the metal phase which leads to reduced surface area and activity. To overcome this issue Pd/Zn was supported on alumina, much like has been done for other catalysts. [12] $Pd/ZnO/Al_2O_3$ with smaller metal particles did prove to have improved surface area stability, but showed lower selectivity to CO_2, and TEM-EDS showed these catalysts contained fcc Pd and ZnO in addition to the tetragonal $PdZn_{b1}$. Since fcc Pd is known to be selective to CO, it was suggested that the lower selectivity was due to catalytic contributions from Pd. In a catalyst that contains a mixture of several phases, it is very difficult to establish correlations between activity, selectivity and phase composition. It is important to determine the effect of added Zn to Pd and whether the underlying bulk structure of such catalysts is important for their catalytic behavior. However, such a study cannot be carried out on supported catalysts, since it is difficult to achieve identical composition in each nanoparticle, and since a typical Pd/ZnO catalyst can contain multiple phases.

We recently reported the aerosol synthesis of phase pure $PdZn_{b1}$ [2] which was then used to study the intrinsic reactivity of this phase for the steam reforming of methanol and CO oxidation[3]. We found that $PdZn_{b1}$ catalyzes MSR with near 100% selectivity to CO_2 with an activation energy of E_A~48kJ/mol, very near the heat of reaction, and TOF at 250 C of $0.21s^{-1}$ which is in line with previously reported TOF values.[11] Since $PdZn_a$ is structurally similar to fcc Pd- and cannot be easily distinguished from Pd by TEM, especially when present on ZnO supports, it is important to know whether the added Zn in the fcc structure plays a similar catalytic role, as is observed for the tetragonal $PdZn_{b1}$ structure.

In previous work [10, 13, 14] it was shown that small amounts of Zn added to Pd(111) change the surface chemistry dramatically. The binding energy of CO dropped significantly even when the coverage of Zn was 3% of a monolayer. At higher coverages of Zn, ordered structures were seen to form and by 50% Zn the Pd(111) surface was essentially inactive towards adsorption of methanol or CO. In light of these observations, it is very relevant to study the steady-state catalytic behavior of samples where similar amounts of Zn that have been incorporated into the Pd bulk. The aerosol synthesis approach allows us to generate metal powders with precisely controlled amounts of Zn that are homogeneously dispersed without segregation into multiple phases as is encountered in other synthesis approaches. In this work we report the synthesis and structure of bulk metal powders with 12%Zn added to Pd to form the $PdZn_a$ phase. Phase pure, uniform composition, metal nanoparticles were synthesized via aerosol synthesis [2] and these metal powders were characterized to determine the intrinsic selectivity and TOF of $PdZn_a$ as well as the bulk and surface structure and stability during MSR.

2. Experimental

2.1. Materials

PdZn aerosol-derived catalysts were made using Palladium and Zinc Nitrate (Aldrich, 99.99%+) dissolved in 10% nitric acid to make a 45mM solution. The nitrate salt mixture was atomized using a commercial nebulizer device(Walgreens Cool Mist Humidifier) to produce droplets that dried as they passed through a furnace operating at 700°C using 1.5LPM N_2 carrier gas with a residence time of approximately 0.1sec, and were collected on a 0.4mm filter. The collected powder was reduced at 500 °C in flowing 5%/95% H_2/N_2 for 4 hours. The reduction temperature was selected based on previous studies for making the PdZn $L1_0$ phase that allow rapid formation of the intermetallic but without significant loss of Zn due to evaporation. This approach is described in detail in a previous study where phase pure $PdZn_{b1}$ was synthesized [2]. The reference Pd powder (Alfa, 99.98%) was calcined in air at 350°C for 3 hours, then reduced at 500 °C in flowing 5% H_2 for 4 hours.

2.2. Characterization

Nitrogen adsorption was measured at 77°K with in a Micromeritics Gemini System, and Quantachrome Autosorb 1-C/TCD. The samples were treated at 120°C for 3+ hrs under vacuum before measurements. The surface areas were determined from adsorption values for five relative pressures (P/P_0) ranging from 0.05 to 0.2 using the BET method.

CO TPD and pulse chemisorption experiments were conducted on a Micromeritics AutoChem II 2920 analyzer. Catalysts (typically 0.1-0.3g) were loaded in a quartz tube that was placed in the built-in furnace. Temperature control was achieved via a type-K thermocouple that was inserted in the quartz tube just above the catalyst layer. The quartz tube was connected to gas lines that were controlled with built-in mass flow controllers. The catalysts were typically purged with dry helium and then reduced in 10% H_2/Ar (total flow 50 sccm) at 400°C for 2 hr before experiments.

For CO TPD experiments, the sample was first saturated with CO and then purged with dry helium to remove physisorbed molecules before temperature ramp (10 K/min from ambient to 500°C). CO desorption was monitored with a built-in TCD detector. For pulse chemisorption studies, the cleaned sample was exposed to pulses of 0.5-ml CO or H_2 until 5 consecutive pulses yielding identical signal areas. CO pulse chemisorption was conducted at 50°C; H_2 pulse chemisorption was performed at 100°C to avoid metal hydride formation.

Scanning electron microscopy (SEM) was performed on a Hitachi S-5200, with a resolution of 0.5 nm at 30 kV and 1.7 nm at 1 kV, EDS was carried out at 20kV using a PGT Spirit system.

X-Ray fluorescence was conducted on Spectrace QuanX EDXRF at 50keV, with 2nm spot size and Zn and Pd standards.

X-ray powder diffraction patterns were recorded using a Scintag Pad V diffractometer with DataScan 4 software (from MDI, Inc.) for system automation and data collection. Cu K_a radiation (40 kV, 35 mA) was used with a Bicron Scintillation detector (with a pyrolytic graphite curved crystal monochromator). Data sets were analyzed with Jade 9.5 Software (from MDI, Inc.) using the ICDD (International Center for Diffraction Data) PDF2 database (rev. 2004) for phase identification. Rietveldt analysis was performed using the software package GSAS[15], employing an anisotropic microstrain model in the peak profile function [16].

X-ray Photoelectron Spectroscopy was performed on a Kratos Axis Ultra X-ray photoelectron spectrometer. Spectra were recorded under the operating pressure of around 2×10^{-9} torr using a monochromatic Al K_a source operating at 300 W with charge compensation. Broad-range spectra were acquired at 80eV pass energy while high resolution spectra were acquired at a pass energy of 20 eV. Ambient Pressure XPS experiments were carried out at ISIS, the catalysis beamline of the Fritz Haber Institute at the 3rd generation synchrotron BESSY II (Helmholtz-Zentrum Berlin). The powder samples were pressed into self supporting discs >0.5mm thick that were mounted in the *in-situ* heated holder and exposed to gases at up to 0.25 mbar. Spectra were generated using incident photon energies of 120eV above monitored B.E. energy window and adjusted for beamline photon flux variations. Incident photon energies were 120eV for Zn3d/VB, 410eV for C1s, 460eV for Pd3d, 650eV for O1s, and 1250eV for Survey scans. Pass energy was 20eV for survey and 10eV for detailed scans, respectively and the exit slit of the beamline was 111mm. The sample was mounted, chamber evacuated, and survey and detailed scans were first acquired. The sample was then heated to 250 °C in the presence of flowing 0.25 mbar (or 0.19 Torr) hydrogen, then MSR reactions were carried out under 1:1 CH_3OH:H_2O at 0.5mbar, sample was cooled to 100°C and 1:1 CO:O_2 fed at 0.5mbar. Reactions were monitored via QMS. Quantification of XPS was performed using CasaXPS software. Subtraction of a Shirley background was followed by charge referencing of all spectra to gold powder dabbed near the sample for ex-situ XPS, carbon at 285 eV, and the Fermi-level. Sensitivity factors were provided by the manufacturer or referenced to published data. Curve-fitting was carried out using individual peaks with 70% Gaussian/30% Lorentzian line shape and widths and binding energies were constrained to best experimental fittings of reference Pd, PdO, and ZnO materials. For conciseness only APXPS results are presented in this manuscript.

2.3. Catalytic activity

All catalysts were pelletized and sieved to 106-260 mm, then 20mg of the sieved powder was loaded in a 1.7mm ID reactor tube with a packed catalyst bed length of ~20mm and ~5mg quartz wool plug on either end of the catalyst bed.

Reactivity studies were performed in a reactor tube placed in a temperature programmable convection furnace for the reactor capable of 30°C/min heating, a reactor feed system, and a Varian 3800 GC equipped with TCD detector for the analysis of the products. The reactor feed system used MKS mass flow controllers and a high pressure pump-fed vaporizer system for introducing liquid reactants such as water and methanol. Samples were treated *in-situ*, and then tested for MSR activity at 250°C until steady state performance was achieved. Oxidation, reduction, and oxidation and reduction treatments followed by MSR at 250°C were used to evaluate the catalyst deactivation and regeneration. Once steady MSR performance was reached, the MSR reactivity was measured over a range of temperatures, followed by CO-oxidation measurements to quantify the surface palladium sites. Methanol steam reforming activity was evaluated using a high-pressure pump that feeds 0.003ml/min of a pre-mixed water/methanol mixture (molar ratio of 1.1:1) aerated with 77.5 sccm preheated Helium through a vaporizer operating at 100°C and introduced directly into the reactor. Prior to activity tests, the catalyst was oxidized in-situ for 60 minutes using 50sccm 2%O_2/He at 250°C to burn off any contaminants then reduced in-situ under 50 sccm 5%H_2/He for 120 minutes at 250°C[17] to reform the alloy at the surface. Product gases from the reactor were analyzed using a series/bypass configured mol-sieve/Capillary column in a Varian CP-3800 GC equipped with TCD detector. CO oxidation was carried out in the same system using flows of 30 sccm 5%CO/He, 50sccm 2%O_2/He.

High vacuum TPD experiments were conducted in a diffusion-pumped system equipped with VGQ quadruple mass-spectrometer, temperature controlled radiatively heated sample basket, cold-cathode gage for pressure measurement, and leak valve for introduction of probe gasses. Approximately 20mg of the powder sample was loaded in the basket, pumped down for 4 hrs, then heated to 350°C in 2 Torr H_2 for 2 hrs to remove adsorbed environmental gasses and rereduce the PdZn alloys. Samples were exposed to 2 Torr probe gas for 30 minutes, and then pumped down for

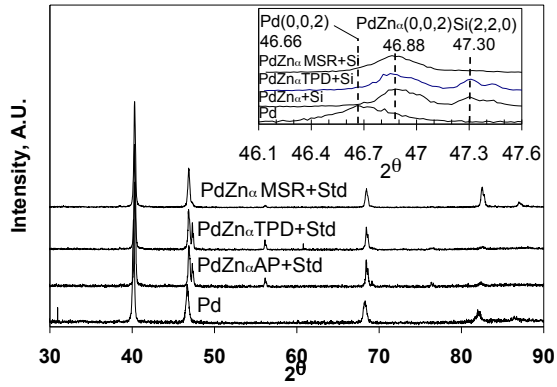

Figure 1 XRD shows a single phase for $Pd_{88}Zn_{12}$ as expected from the metallurgical phase (Pd, Zn) phase diagram. AP – as prepared, MSR – after methanol steam reforming, TPD – after temperature programmed desorption.

4 hrs. Samples were then heated at 10K/min up to 427°C and desorption products monitored by quadruple mass-spectrometer. Standard analysis adjusting for overlapping fragmentation patterns was applied.

3. Results

X-Ray Diffraction is presented in Figure 1, the spectrum for Pd shows peaks at 40.78, 46.66, 68.36, and 82.13 2q in agreement with ICDD card number 046-1043. To allow for accurate analysis $PdZn_a$ was mixed with NIST Si standard 640b, and sample displacement was adjusted to the internal Si standard. The diffraction peaks for $PdZn_a$ (111), (200), (220), and (311) are 40.30, 46.88, 68.44, and 82.36. The absolute position of the $PdZn_a$(0,0,2) is confirmed by comparison to the Si(2,2,0) internal standard at 47.3, shown in the inset expanded region. Refinement of the $PdZn_a$ yields a cell constant of 3.866Å, a 0.6% shrinkage of the lattice constant versus Pd and consistent with substitution of Pd with smaller Zn atoms. Patterns of the as prepared, and the samples used for TPD and MSR studies show that the bulk structure of the $PdZn_a$ is unchanged after reaction testing. Scherrer analysis yields an average crystallite size of 47nm.

3.1. Surface area and composition

Surface area and composititon were determined via BET, Chemisorption and XRF. BET surface area of the $PdZn_a$ sample is determined to be 1.31±0.04 m^2/g. Pulse chemisorption of $PdZn_a$ established CO uptake to be 0.29cc/g which translates to 1.25m^2/g using 7.94Å per Pd[18] and a bridge bonding arrangement for CO.[14, 19-21] XRF measurements determined the composition of the PdZn to be 88.6±0.1at%Pd and 11.4±0.1at%Zn.

3.2. SEM/EDS

SEM/EDS micrographs displayed in Figure 2 demonstrate that the aerosol-synthesis process produces irregular aggregates composed of sintered particles. The aggregate diameters are on the order of 500 nm and the sintered particles 20-70nm. Based on the XRD and chemisorption data, we infer that these aggregates are composed of 20-60 nm irregularly shaped particles and grains and some less well intercalated particles of the same size. The observed SEM/EDS composition of the aerosol-derived powders is 87±3at% Pd.

3.3. TEM

TEM structural and compositional analysis of $PdZn_a$ after MSR testing are displayed in Figure 3. Figure 3A is a HRTEM micrograph showing crystalline lattice fringes extending all the way to the surface of a thin section. Inset FFT is indexed to fcc Pd (2,0,0) and Pd(1,1,1) planes in agreement with a grain that is tilted off the [0,1-1] zone axis, demonstrating that the used $PdZn_a$ maintains its fcc structure. A STEM image and superimposed STEM/EDS compositional linescan in Figure 3B demonstrate uniform composition across the used $PdZn_a$ crystallite.

3.4. Ambient Pressure XPS

Ambient pressure XPS composite spectra for a $PdZn_a$ sample made from pressed powder then mounted in the AP-XPS system at Bessy II is displayed in Figure 4. Sample composition through out the experiments is displayed in Figure 5. The sample was mounted, heated in vacuum to 250°C, reduced in flowing hydrogen, exposed to 1:1 CH_3OH:H_2O, and then to 1:1 CO:O_2. Survey scans showed only Pd, Zn, C, and O in the sample throughout the experiments. High resolution scans were conducted using incident photon energies that are 120eV above the measured emission peaks to maintain a constant sampling depth of less than 1.0 nm based on an estimated 0.67nm effective mean free path for 120eV photoelectrons.[22] Measurements to monitor spectra changes under reactive gas atmosphere were conducted at a constant 650eV incident photon energy to allow for more rapid measurement. The calculated inelastic mean free path(IMFP) and transport mean free path(TMFP) for $Pd_{88}Zn_{12}$ at 120eare tabulated in Table 1.

The Pd3d peak assignments were based on metallic Pd at 335.1eV, metallic to oxide shift of 1.6eV to higher binding energy at oxygen mbar pressure range[23, 24]. Studies using the same instrument used in this current study also reported 0.8eV upward [10, 25] shift for bulk and 0.4eV shift for monolayer PdZn, in agreement with other studies that included analysis of PdZn/ZnO powders and single crystals[6, 26-28]. Using these values it appears that the Pd in this sample is metallic and possibly as much as

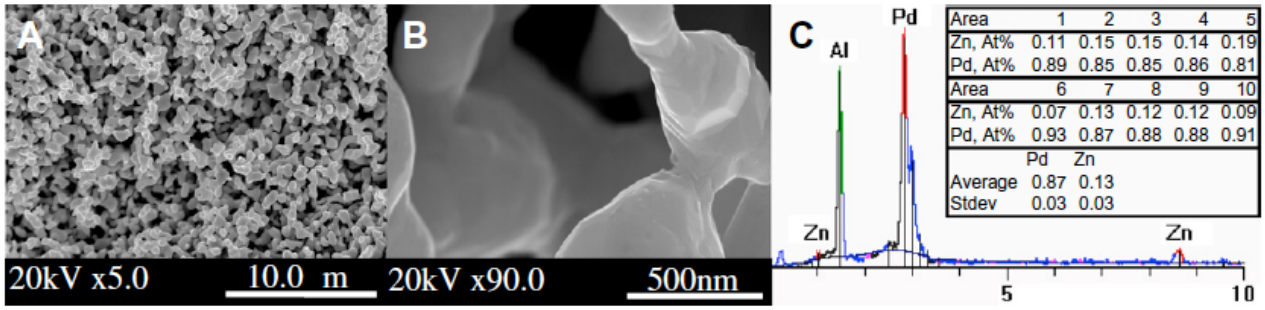

Figure 2 SEM micrographs, A) and B), of the $PdZn_a$ samples show a powder composed of 500nm sintered agglomerates. C) SEM/EDS gives compositions of 87±3At%Pd.

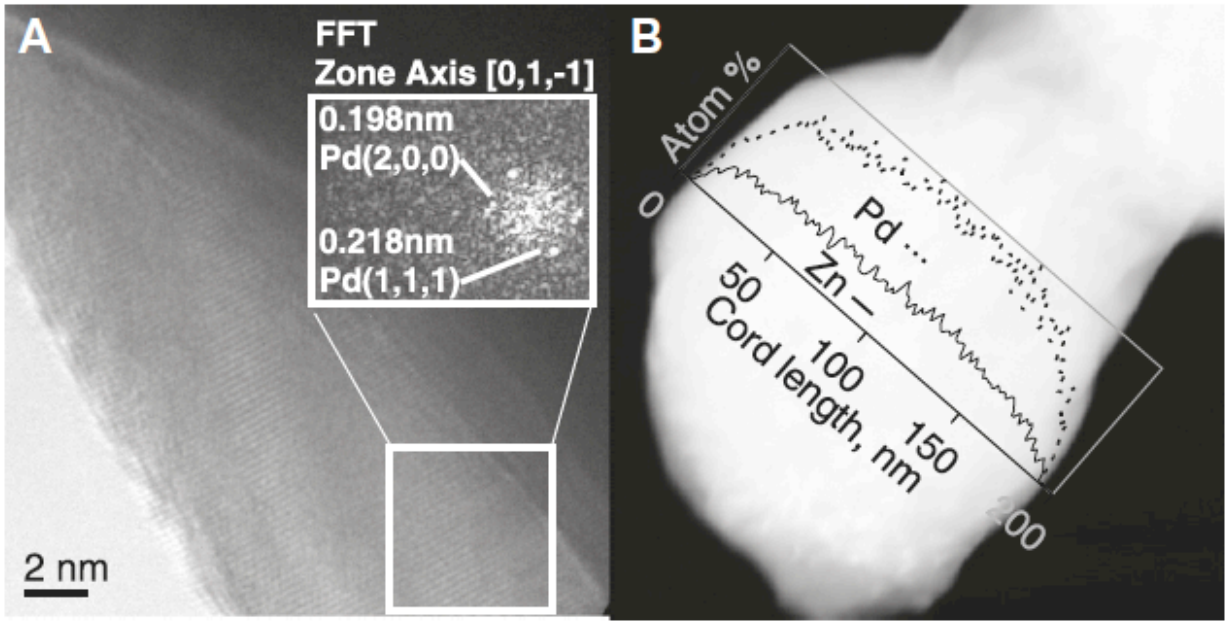

Figure 3 TEM structural and compositional analysis of $PdZn_a$ after MSR testing. A) HRTEM showing nanocrystalline lattice fringes extending to the surface of a thin section. Inset FFT is indexed to fcc Pd (2,0,0) and Pd(1,1,1) planes in arrangement corresponding to [0,1-1] zone axis. B) STEM and superimposed STEM/EDS compositional linescan demonstrates uniform composition across the used $PdZn_a$ crystallite.

10% is alloyed with Zn. More importantly, the shape and position of Pd3d does not change under different conditions except for slight change in the Pd3d peak shape, indicating a small degree of oxidation under CO-oxidation conditions.

The data available for high resolution analysis of Zn3d is sparse, however there are several studies utilizing synchrotron based XPS that can be used as a reference. Metallic Zn has been reported to have BE values ranging from 9.1[10, 25] to 9.9eV[29] or even 10.2[30]. For the purposes of analysis the value of 9.1 is used here because it was obtained on the same instrument used for this study. These same studies on the AP-XPS system at BESSY II also found that monolayer PdZn appears at 9.15 while multilayer PdZn occurs at 9.6[10, 25] and the Zn3d doublet peak separation is roughly 0.3. [10] The metallic to oxide shift reported is more consistent, showing a 0.7-0.9eV shift [10, 25, 29, 31, 32] to higher binding energies, where a monolayer of ZnO has a shift of 0.4eV[33]. Determination of the oxidation state of Zn3d is further complicated by overlapping spectra of the CO gas fed under AP-XPS conditions which appear at 9.6eV and were measured directly during the study. The raw data, CO background, and Zn3d/CO composite peak after CO subtraction for Zn3d under CO-Oxidation conditions are included in the spectra. Analysis of the Zn3d spectra indicate the presence of three peaks with BE of 9.1, 9.4, and 9.55eV. The peaks at 9.1 and 9.4 correspond to metallic Zn with appropriate doublet separation. Some oxide is evident in the sample initially but is removed under reduction. The Zn3d peak then remains essentially constant under both MSR and CO-Oxidation reactions, with perhaps as much as 10% growth of oxide after CO-Oxidation experiments.

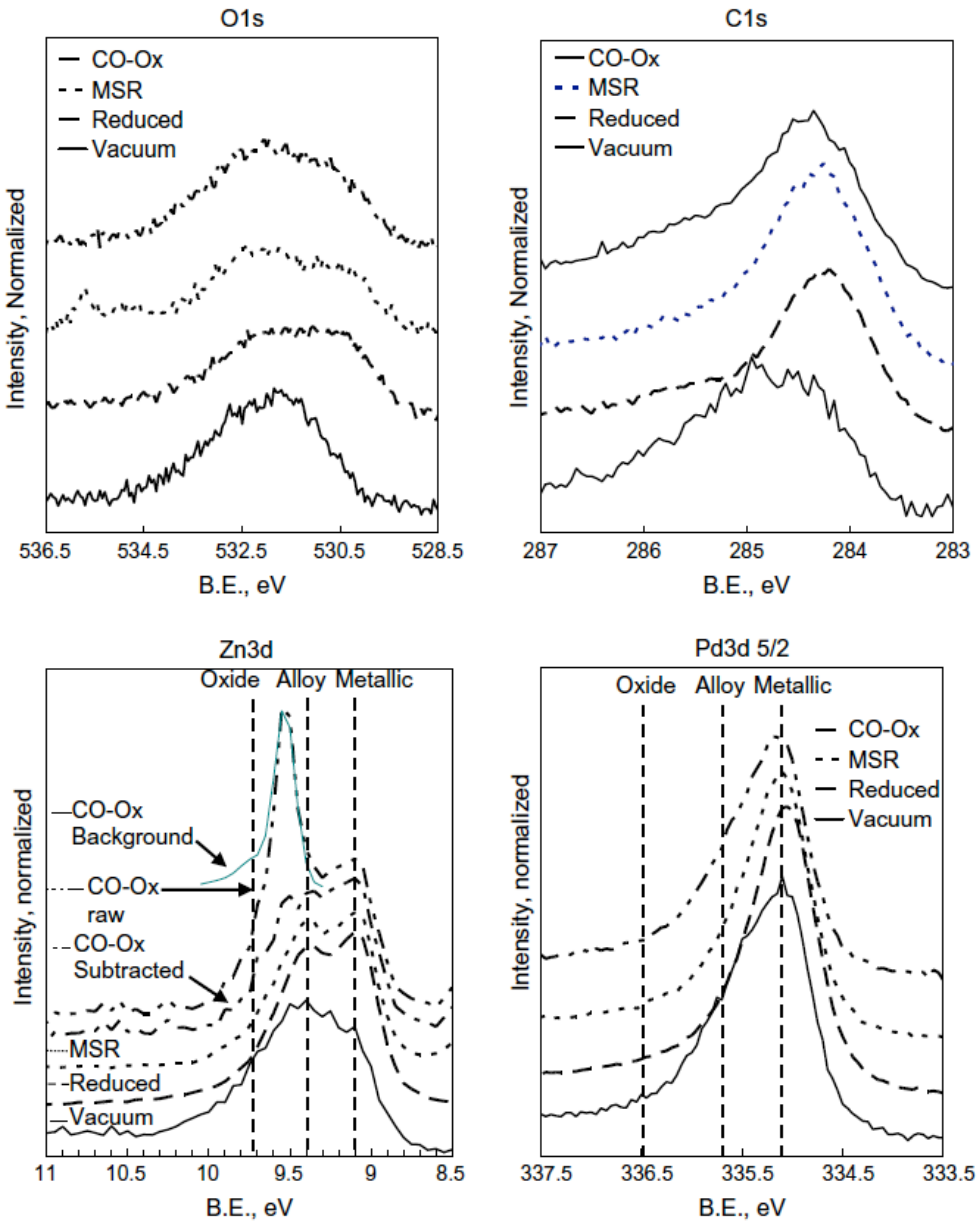

Figure 4: AP-XPS composite spectra for O1s, C1s, Pd3d, and Zn3d captured at 5eV pass energy and incident photon energy was set so the kinetic energy of monitored features is 120eV to ensure constant sampling depth. The Fermi level was monitored to evaluate sample charging and none was observed.

The O1s spectra have two main features at 531.5 and 530.2eV, corresponding to metal oxide and adventitious origins. Pd3p at 533eV was subtracted from the plotted O1s using a 3:1 Pd3p:Pd3d ratio. Once the adventitious oxygen is removed after heating the O1s peak shape remains largely unchanged through out the reactivity experiments. C1s spectra show some adventitious carbon loss after heating, and a main peak at 284.3 which is essentially unchanged throughout the experiment and indicates either the presence of carbide or background contamination typical to AP-XPS systems.

3.5. Temperature Programmed Desorption

Temperature Programmed Desorption of CO in vacuum, Figure 6, normalized to sample surface Pd content shows that CO dosed desorbs from Pd, $PdZn_a$, $PdZn_{b1}$ in 3 main temperatures 530, 450, and 420 with peak areas in dropping in the following proportion 11:9:1. Minor peaks are also observed for Pd and $PdZn_a$, at 400 and 530K. Since CO adsorption does not occur on Zn the integrated area of desorbing CO provides a measure of the surface Pd area.

TPD experiments were also used to monitor the decomposition of methanol, Figure 7, with desorption

Table 1 Calculated inelastic mean free path(IMFP) and transport mean free path(TMFP) for $Pd_{88}Zn_{12}$.

KE (eV)	IMFP (nm)		TMFP (nm)	
	Pd3d	Zn3d	Pd3d	Zn3d
120	0.66	0.66	0.68	0.68
315	1.03		1.06	
640		1.69		1.85

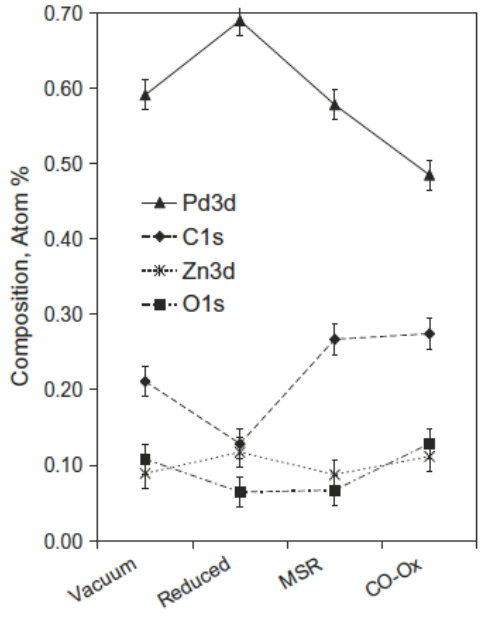

Figure 5 Surface composition summary based on the AP-XPS spectra for O1s, C1s, Pd3d, and Zn3d.

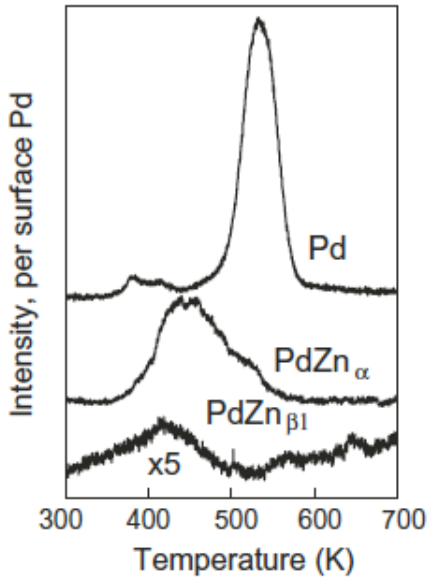

Figure 6 Vacuum Temperature Programmed Desorption of CO dosed on powder Pd, $PdZn_a$, and $PdZn_{b1}$. Signal Intensity is scaled to surface Pd content which is estimated from BET and nominal composition, and confirmed by chemisorption. The product from $PdZn_{b1}$ is magnified by 5 for clarity.

products, temperatures, and derived Redhead analysis desorption energies summarized in Table 1. All three samples showed similar product, with different desorption temperatures and amounts. For Pd, $PdZn_a$, and $PdZn_{b1}$ methanol desorption is observed at 405, 430, and 470°K; while formaldehyde appears at 430, 530, and 570°K; and CO at 530, 470, and 630°K. A summary of desorption temperatures and Redhead analysis-derived desorption energies is in Table 2.

3.6. Microreactor MSR Reactivity

After *in*-situ pretreatment, the bulk $PdZn_a$ was tested for MSR and CO-oxidation. The catalytic performance illustrated in Figure 8 shows a typical catalyst test that lasted over several days wherein the MSR reaction runs were alternated with *in-situ* CO-oxidation. Shorter activation treatments consisting of 15-30 minutes of oxidation/reduction at 250°C were compared to 60-120 minutes oxidation/reduction activation treatment of the catalysts. The shorter pretreatment proved insufficient to achieve full MSR activity so the longer pretreatment was used in all subsequent experiments. The long term reactivity tests show deactivation of $PdZn_a$ under MSR reaction conditions at 250°C. MSR selectivity was 100% to CO from 170-270°C. To test for induction time when switching between MSR and CO-oxidation the GC product sampling occurred within 1 minute of switching the reactor feed. Interestingly, there is no observed induction time for catalyst performance when switching the reaction mixture from CO-Oxidation back to MSR. The results of switching between CO-oxidation and MSR show that the CO oxidation measurements in fact served to regenerate the catalyst. Burn-off experiments, where catalyst used for MSR was exposed to O_2 at 250°C, showed CO_2 evolution confirming that the deactivation observed for $PdZn_a$ is likely due to coking. Additional experiments were conducted with a doubled catalyst amount, configured so that the catalyst bed length was doubled, the TOF results of these experiments are summarized in Fig 9. These increased catalyst loading experiments confirmed that transport limitations were not greatly affecting the observed reaction rate, where the increased catalyst loading requires higher flow rates for similar conversion, and a faster rate of mass transport.

Reports of MSR performance on Pd were not found in the literature so an unsupported commercial Pd powder was similarly tested for MSR. The unsupported Pd was found to be 100% selective to CO under MSR conditions and deactivated due to coking.

The surface palladium atom concentration (24mmol Pd/gr_{sample}) was used to calculate the turnover frequencies (TOF) in Figure 9. TOF for $PdZn_a$ is therefore $0.12s^{-1}$ for MSR at 250°C and $0.075s^{-1}$ for CO-Oxidation at 170°C. Arrhenius analysis yields 52±2kJ/mol apparent activation energy for production of CO from Methanol and Water on $PdZn_a$. The apparent increase in activation energy for the data obtained from a doubled catalyst load is approximately

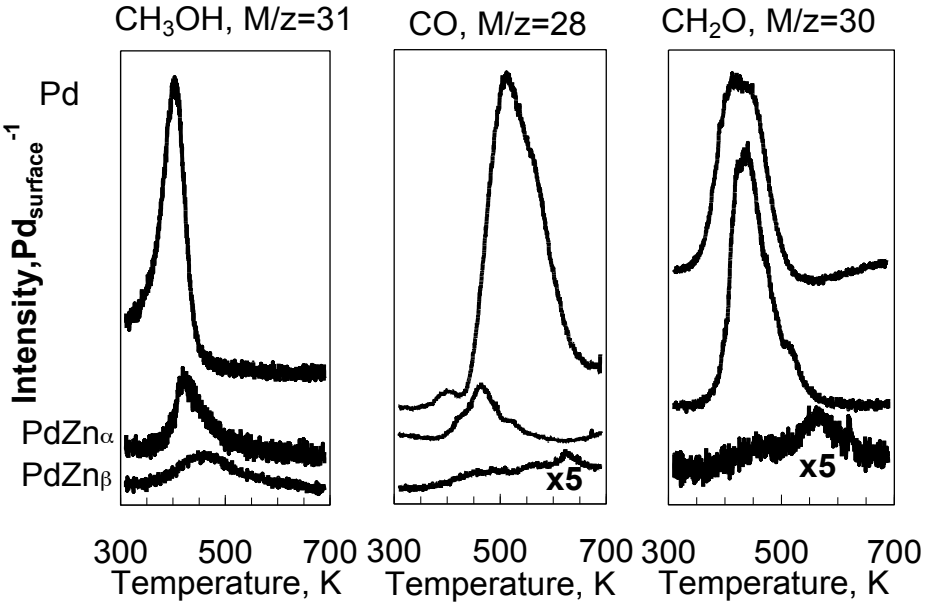

Figure 7 Vacuum Temperature Programmed Desorption of CH_3OH dosed on powder Pd, $PdZn_a$, and $PdZn_{b1}$. Signal Intensity is scaled to surface Pd which is measured by pulse CO chemisorption and confirmed by BET and XPS determination of surface composition. The CH_2O and CO products from $PdZn_{b1}$ are magnified by 5 for clarity.

Table 1 TPD desorption product and energies for CO and CH_3OH dosed on Pd, $PdZn_a$, and $PdZn_{b1}$. Signal Intensity is scaled to surface Pd content which is estimated from BET and nominal composition, and confirmed by chemisorption.

		Pd		$PdZn_{\alpha}$		$PdZn_{\beta 1}$	
Probe	Product	T_{des}, K	E_{des}, kJ/mol	T_{des}, K	E_{des}, kJ/mol	T_{des}, K	E_{des}, kJ/mol
CO	CO	530	150	450	125	420	120
CH_3OH	CH_3OH	405	115	430	122	470	1
CH_3OH	CH_2O	430	122	530	152	570	164
CH_3OH	CO	530	152	470	134	630	181

8%. For the commercial unsupported Pd the apparent activation energy of 29 kJ/mol and TOF of $0.015s^{-1}$ were determined for the CO formed under MSR conditions. For comparison purposes the performance of $PdZn_{b1}$ which was reported previously[3] is plotted along with the results obtained for $PdZn_a$ and Pd in this study.

4. Discussion

4.1. Surface area and structure

XRD Rietveldt refinement shows a 0.6% contraction in the unit cell dimension compared to pure Pd with a = 3.89019 Å (ICSD), consistent with contraction due to the smaller size of the Zn added to the Pd FCC lattice. The diffraction-estimated crystallite size for the aerosol-derived PdZn suggests a surface area of $11m^2/g$ based on an assumption of spherical particles.[18] The measured BET surface area is a much lower at 1.3 m^2/g after sieving. It is therefore clear that each particle is composed of multiple crystallites and hence the XRD-average crystallite size cannot be used for estimating the available surface area of the unsupported PdZn. SEM observations also show that the $PdZn_a$ powder is composed of spherical sintered agglomerates, as expected from spray pyrolysis. Since both BET and chemisorption measurements are in good agreement all TOF calculation used the BET measured surface area of $1.3m^2/gr$ and 88at%Pd thus leading to a calculated surface of 24 mmole surface Pd per gram of catalyst. HRTEM demonstrates that the $PdZn_a$ maintains fcc structure without evident formation of ZnO overlayers. Further, STEM/EDS elemental composition linescans demonstrate uniform composition across crystallites. However, the 1nm diameter beam needed to produce sufficient counts for EDS analysis and multiple X-Ray scattering that can occur in such thick and dense crystallites limit the spatial resolution of the STEM/EDS results so that the true composition of the outer 1-3 nm is not accurate. However, within the measurement limits the sample composition is stable even after days of operation suggesting the $PdZn_a$ structure and composition is stable under MSR

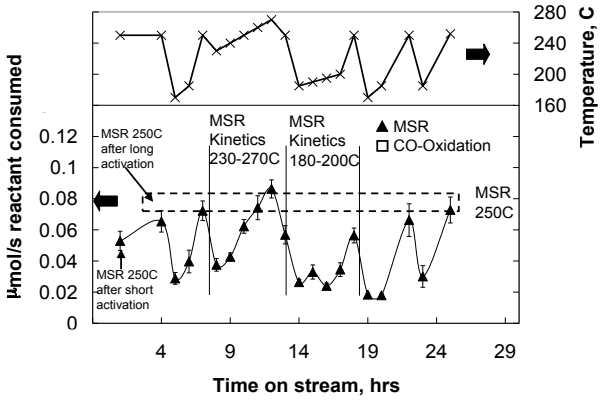

Figure 8 On-stream catalytic performance of PdZn alpha under MSR(Δ) and CO-Oxidation(□). Dashed line illustrates MSR performance envelope at 250 °C over time. The reactor temperature was changed over the course of this extended run to alternately perform CO oxidation and MSR reactivity measurements on the same catalyst. As shown here, there is little induction time after switching from CO-oxidation to MSR reactivity, whereas CO oxidation is able to burn off carbon and reverse the modest deactivation observed at 250 °C during MSR.

4.2. APXPS Ambient Pressure-XPS

After reduction the sample is composed of 80at% metallic Pd and Zn, with 20at% carbon and oxygen. The small amount of oxygen in the sample after reduction and the small amount of metal-oxides observed suggest that the oxygen observed after reduction results from a combination of system contamination, metal oxide, and carbonyls. While the metallic oxide content is at most 10%, it is unlikely that exposure to MSR gas mix increases the oxygen content slightly while remaining constant over the 1 hr duration of the experiment- indicating a possibility of sub-monolayer surface hydroxylation, surface oxidation, or system contamination.

Upon exposure to MSR, carbon content doubles to 27%, while oxygen remains constant at 7% and the ratio of Pd to Zn is maintained. Combined with the nature of the C1s peak this suggests the formation of a carbide layer under MSR. The carbon content is retained during CO-oxidation, while oxygen content doubles and zinc increases slightly. These changes and the slight growth of oxide seen in the Pd3d peak suggest that the excess oxygen in the CO-oxidation mix serves to oxidize the carbide to oxide and perhaps pull Zn to the surface as well, although the formation of ZnO is not seen in the noisy Zn3d spectra. MS analysis of the chamber effluent during AP-XPS matched micro-reactor studies where CO was the main product under MSR and CO_2 the main product during CO-oxidation conditions. Thus it is clear that while the bulk material is unchanged under AP-XPS conditions, build up of carbon and oxygen consistent with carburization and then oxidation of 1-2 surface layers is observed under MSR and CO-oxidation conditions. These surface layers build within minutes of exposure to reactive gases, but then are stable over the 60 minute duration monitored. Since micro-reactor studies show deactivation due to coke formation, it is reasonable to extrapolate that longer APXPS experiments would show similar deactivation.

The Pd:Zn ratio under all conditions is higher than nominally expected, suggesting either a surface depletion in Zn or inaccuracies in the factors used in quantification. The slight increase in Pd:Zn ratio suggests that the heating used served to somewhat volatilize some of the surface Zn. MSR and CO-oxidation then serve to decrease the Pd:Zn ratio, perhaps by drawing Zn from the bulk to the surface. However, under all conditions the shape of Pd and Zn are relatively invariant, indicating that the chemical nature of Pd and Zn remain constant under reaction conditions even while some change in surface Pd:Zn ratio are dynamic. The slight change in the Pd3d peak shape under CO-oxidation indicates only a small degree of Pd oxidation, lending support to our approach of using CO-oxidation as an *in-situ* method for quantifying active Pd catalyst surface area.

4.3. Temperature Programmed Desorption

4.3.1. CO

Redhead analysis of the desorption peaks is presented in Table 6. The desorption, and therefore likely binding energies are 150, 125, and 120 kJ/mol for CO on Pd, $PdZn_a$, and $PdZn_{b1}$ While quantitative analysis of TPD is inaccurate for powder samples, the large disparity in adsorbate amount between $PdZn_{b1}$ and $PdZn_a$ is illustrated by the total amounts of CO that adsorbed. For reference purposes the BET surface areas of the sieved $PdZn_{b1}$ sample is $2.9 m^2/gr$ with 0.32 cc CO chemisorbed, and for the commercial Pd sample BET is $4.77 m^2/gr$ with 0.54 cc H_2 chemisorbed. Note that expected surface Pd content estimated from the BET and bulk composition of the samples is confirmed within 10% by the chemisorption results if a bridging position is assumed for CO on PdZn alpha and beta alloys.

The much smaller amount of CO adsorbed on $PdZn_{b1}$ when compared to $PdZn_a$ illustrates the poisoning effect Zn has on CO binding sites. In contrast, the coverage areas for Pd and $PdZn_a$ are sufficiently similar to be consistent with their relative Pd content, indicating similar binding sites. The decrease in CO desorption temperature with increased Zn content illustrates that addition of Zn to Pd serves to weaken CO binding to Pd. Further, since the CO desorption energies for $PdZn_a$ and $PdZn_{b1}$ are similar, it is evident that the effect of Zn addition to Pd on the binding energy of CO saturates near 12%Zn. The 12% Zn represents a nearly the statistical average for every Pd having on average 1 nearest neighbor Zn, therefore suggesting that the maximum effect of Zn on CO-Pd binding is achieved from a single Zn neighboring Pd.

These results are comparable to previously reported UHV CO TPD experiments conducted on PdZn alloys

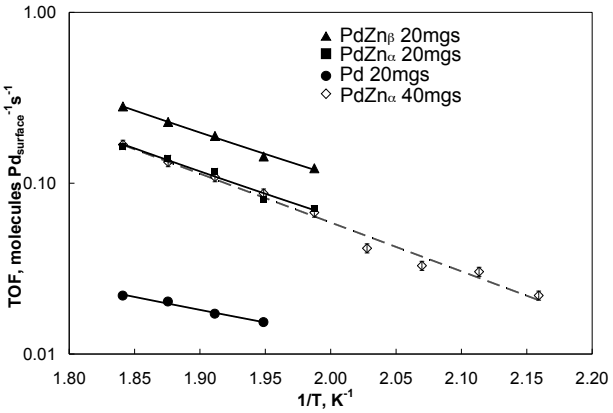

Figure 9 Turnover Frequency (TOF) for reactant molecules consumed under MSR per surface Palladium atom. Surface Palladium atom determined by CO chemisorption and confirmed by BET/XPS. Two data sets are plotted for $PdZn_a$ with 20 and 40mgs of catalyst used in the packed bed reactor. Data point indicators are larger than the measurement error so are only explicitly shown for the 40mgs $PdZn_a$ data set.

formed from Zn/Pd(111) [14]. In these experiments it was observed that increasing amounts of Zn deposited on Pd(111) reduced both the amount of CO adsorbed and the temperature of desorption for CO. In the single crystal work it was also found that CO desorption occurred well below room temperature when more than 0.25ML Zn was deposited to make a 75at%Pd 25at% Zn surface alloy. On the powder samples presented in this study CO desorbed above room temperature for the $PdZn_{b1}$ sample which contains more than 25at% Zn at the surface. In addition to the differences in CO binding on powder and single crystal Pd-based materials DFT studies indicate a 100kJ/mol difference in CO adsorption between Pd and $PdZn_{b1}$(111), not the 30kJ/mol observed for the powders in this study. It is therefore possible that the differences observed between CO desorption from Zn/Pd(111) and PdZn bulk powder alloys are due to the vastly increased dosing pressure used on the powder samples or that the sites created by deposition of Zn on Pd(111) are not be the same as the sites present on bulk PdZn alloys. At the same time, it has also been shown recently that monolayer alloys can differ in their catalytic behavior from multilayer alloys [10, 34] and from the results reported here, it appears that bulk metal powders may be even different from multilayer alloy films. CO adsorption/desorption experiments on powders therefore qualitatively match both single crystal and DFT experiments, but differ in binding energies reported. However, there are indications in the literature that these disparities may be due to the different behavior of the bulk alloys and atmospheric pressures used in this study, versus the thin film and UHV pressure used in previously reported experiments.

4.3.2. Methanol

The three desorption products observed for methanol decomposition TPD are consistent with a reaction pathway where methanol adsorbs dissociatively to form adsorbed methoxide and hydride. The methoxide can recombine with hydride and desorb as methanol, undergo dehydrogenation to formaldehyde, or further decompose to CO. In the presence of adsorbed hydroxyls formaldehyde can also form formate which can decompose to CO_2. The relatively high desorption energies observed suggest that all three desorption products are reaction limited[8], and therefore can be assigned activation/reaction energies corresponding to the desorption energies. Also, while it was not possible to monitor hydrogen evolution readily by the QMS in this experimental system, comparison to single crystal experiments suggest that the formaldehyde product is formed by dehydrogenation of methoxide.[8, 35]

The methanol desorption product appearing between 400-470 ^oK is most likely a product of methoxide hydrogenation. The increase in observed desorption temperature for this product as a function of Zn added to Pd suggests that Zn addition to Pd hinders either CH_3O-Pd or Pd-H bond breakage. As DFT has shown Zn addition to Pd strengthens Pd-OCH_3[35] bonds it is likely that breaking the Pd-CH_3O is therefore the rate limiting step in the rehydrogenation of methoxide to CH_3OH.

As the CO products from methanol decomposition appear at temperatures higher than are seen for CO TPD the observed CO desorption temperatures must be reaction limited. Zn addition to Pd therefore retards the full decomposition pathway. At the same time, the addition of Zn stabilizes the formaldehyde to higher temperatures and simultaneously allows for stabilization of hydroxyls.[36] The stabilization of formaldehyde eventually causes the formaldehyde product to appear at a temperature that is lower than the CO product. DFT predictions help identify step-like defects as the likely sites for formaldehyde adsorption, since formaldehyde adsorbed more strongly on the stepped PdZn(221) surface than on PdZn(111)[36]. Thus formaldehyde is the preferred product from methanol decomposition on $PdZn_{b1}$ while CO is preferred on Pd and $PdZn_a$. The reaction pathway for methanol decomposition on PdZn is therefore consistent with that previously suggested reaction mechanisms [8, 11, 37] where in the absence of water methanol adsorbs to make methoxide, dehydrogenates to make formaldehyde or formate, and further dehydrogenates to CO. The addition of Zn to Pd then serves to stabilize the formaldehyde producing pathway, until it become dominant for $PdZn_{b1}$ so that formaldehyde can be hydrated by hydroxyl during MSR allowing for full oxidation to CO_2.

Briefly, the overall observed desorption products for $PdZn_a$ are consistent with previously suggested pathways in Figure 9[8, 11, 37] for Pd where methanol adsorbs dissociatively to methoxide, which decomposes to formaldehyde, which further decompose and desorbs as CO. The Zn added to Pd serves to strengthen Pd-OCH_3 and weaken Pd-

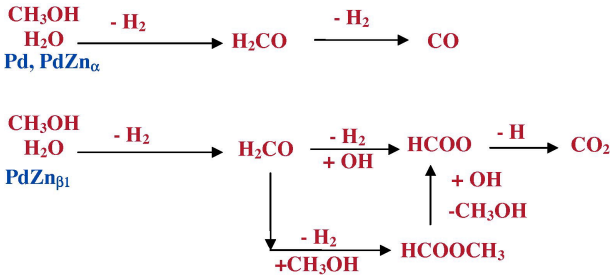

Figure 10 Turnover Frequency (TOF) for reactant molecules consumed under MSR per surface Palladium atom. Surface Palladium atom determined by CO chemisorption and confirmed by BET/XPS. Two data sets are plotted for $PdZn_a$ with 20 and 40mgs of catalyst used in the packed bed reactor. Data point indicators are larger than the measurement error so are only explicitly shown for the 40mgs $PdZn_a$ data set.

CO. For $PdZn_{b1}$ methanol desorbs to methoxide, which decomposes to formaldehyde which can desorb or react with hydroxyl to formate, which can then further decompose and desorb as CO_2. Combining DFT and the current TPD results suggests that Zn addition to Pd serves multiple functions providing for a Pd-like reaction pathway with a branching off when water is co-adsorbed. In the main Pd-like path Zn addition to Pd serves to hinder methoxide re-hydrogenation, reduce Pd-CO binding strength, and shift the RLS of methanol decomposition from methoxide decomposition to formaldehyde to the subsequent formaldehyde decomposition/hydroxylation to formate. Further, Zn addition allows for binding of water and provides hydroxyls that are very stable in 3-fold hollow sites on PdZn and therefore allow for the hydroxylation of formaldehyde to formate which then allows for the production of CO_2.

4.4. Micro-reactor MSR and CO oxidation studies

4.4.1. Deactivation under MSR

While $PdZn_{b1}$ was found to be very stable under MSR conditions, $PdZn_a$ lost ~30% of activity over 6 hrs and then became stable. The deactivation can be attributed to coking based on the reactivation seen after CO-Oxidation and the observance of CO_2 evolution when dilute O_2 was fed to the reactor after MSR performance loss and subsequent MSR performance restoration. Pd showed similar coking behavior.

4.4.2. Reactivity analysis

Arrhenius analysis shows observed activation energies on $PdZn_a$ are 50kJ/mol for MSR with 100% selectivity to CO. TOFs are $0.12s^{-1}$ for MSR at 250°C and $0.075s^{-1}$ for CO-oxidation at 170°C. No other reports on the activity $PdZn_a$ are available. Because reports of MSR activity on unsupported Pd were not found in the literature an unsupported commercial Pd powder was tested for MSR. The unsupported Pd was found to be 100% selective to CO under MSR conditions and deactivated rapidly over several hours. The deactivation was confirmed to be due to coking as dilute oxygen fed to the reactor after catalyst deactivation lead to the evolution of CO_2 and a reactivation of the Pd. It was however possible to measure TOF of $0.015s^{-1}$ and E_a of 29 kJ/mol for the CO formed under MSR conditions on Pd. CO-oxidation on the unsupported Pd was found to have Ea of 87kJ/mol and TOF of $0.027s^{-1}$ at 170°C. These values indicate improved CO-oxidation performance for the unsupported Pd powder when compared to reported Pd/SiO_2[38] where energy of activation of 103kJ/mol and TOF of $0.032s^{-1}$ at 177C, interpolated to $0.02s^{-1}$ at 170°C. The difference in measured activity is unclear, but may be due to the inherent inaccuracies in the quantifying of metallic surface area for supported Pd. It is also possible that the high surface area supports used in the previous study caused mass transport limitations which the low surface area unsupported Pd used in this study did not encounter.

Previous work using the same approach as this current study found that $PdZn_{b1}$ powders catalyze MSR with E_a~48kJ/mol and TOF at 250 °C of $0.21s^{-1}$ while for CO-Oxidation E_a is 78kJ/mol and TOF at 170°C is $0.053s^{-1}$.[3] The similar CO-oxidation TOF values for the two PdZn phases confirm the validity of the approach where CO-oxidation is used in situ to quantify the surface Pd sites for PdZn under MSR conditions. Also, the higher rates of CO-oxidation on PdZn when compared to Pd are consistent with Pd-CO bond breaking being the RLS for CO-Oxidation, since the CO is more weakly bound on PdZn than Pd[3, 39]. Zn may also serve to reduce coking on Pd, through disruption or oxidation of carbonaceous material formed under MSR feed, but this has not yet been sufficiently studied. It is however unclear why the activation energy for MSR on the alpha and beta phases are so similar when the reaction products, and the suggested reaction mechanisms, are so different for the two materials. One possibility is of course good Reverse Water Gas Shift(RWGS) activity on $PdZn_a$. However, tests confirm that $PdZn_a$ is not active for either RWGS or WGS under the conditions used for MSR in this study. To better understand these issues it is useful to examine the likely reaction pathway for the reaction as proposed and supported by several published studies.[4, 8, 11] Since this current study is the first to explicitly make and test $PdZn_a$ it is now possible to lump $PdZn_a$ in the same methanol decomposition pathway as Pd. Examination of the likely reaction pathways reveals that the two PdZn phases share two common elementary reaction steps, adsorption to methoxide and dehydrogenation of the methoxide to aldehyde. While a recent DFT study suggests that adsorption is the RLS for MSR on $PdZn_{b1}$[37], the vacuum TPD showed dissociative adsorption of methanol occurs at room temperature. Therefore the RLS for MSR on $PdZn_a$ must be dehydrogenation of methoxide to formaldehyde. Thus, methoxide dehydrogenation

Table 3: MSR performance summary

	$PdZn_{\beta 1}$	$PdZn_{\alpha}$	Pd
MSR Ea, kJ/mol	48	50	26
MSR TOF @ 250°C, s^{-1}	0.21	0.12	0.015
MSR Selectivity	98%+ CO_2	100% CO	100% CO
CO-Ox, kJ/mol	78	65	87
CO-Ox TOF @ 170, s^{-1}	0.053	0.075	0.027

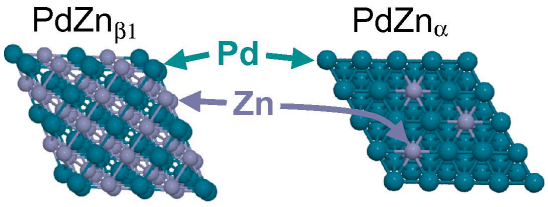

Figure 11 Schematic illustration of PdZn(111) beta and alpha phase structure, from a top-down perspective. Evident is the alternating Pd and Zn "stacked sheet" structure of the beta phase and random Zn-substitution of the Pd fcc lattice in the alpha phase.

to formaldehyde is the likely rate limiting step for MSR on $PdZn_a$. Further, since the vacuum TPD shows very similar product distribution and desorption temperatures on Pd and $PdZn_a$, it is likely that Pd and $PdZn_a$ share the same methoxide dehydrogenation RLS as well. Further support for this hypothesis is derived from the desorption temperatures of the formaldehyde product arising from methanol decomposition. The desorption energies, Table 2, are 122, 152, and 164kJ/mol for Pd, $PdZn_a$, and $PdZn_{b1}$. Thus methoxide dehydrogenation to formaldehyde is most facile on Pd, and this ease of dehydrogenation can help explain the lower activation energy for MSR on Pd when compared to PdZn. The addition of Zn to Pd then serves to weaken the Pd-CO binding energy, as shown in the CO TPD experiments, thus leading to the increase in TOF observed for PdZn when compared to Pd.

The shift in overall product selectivity and reaction pathways can be explained in terms of the energies of formation of the formaldehyde and CO products which arise from methanol decomposition. On Pd and $PdZn_a$ CO is made at lower temperatures than formaldehyde, while on $PdZn_{b1}$ formaldehyde is formed before CO. Thus in steady state experiments methanol decomposes to formaldehyde on $PdZn_{b1}$, which can react with water or hydroxyls to make CO_2. On Pd and $PdZn_a$ decomposition to CO is more facile so that the formate hydro-oxidation pathway is bypassed. The proposed reaction pathway map is illustrated in Figure 10.

5. Summary and conclusions

To understand the inherent reactivity of PdZn phases a 12at%Zn $PdZn_a$ powder was synthesized using a spray-pyrolysis technique. APXPS experiments determined that the surface chemical state of the powder $PdZn_a$ remained constant under constant under MSR and CO-Oxidation AP-XPS conditions. Also, while ZnO was never observed, surface Zn content increased under oxidative conditions and decreased under reductive conditions. Micro-reactor studies showed that $PdZn_a$ MSR selectivity is 100% to CO and TOF at 250°C is 0.12^{s-1}. Steady state ambient pressure MSR and vacuum TPD methanol decomposition experiments showed not only that the alpha phase behaves like Pd, but also that Zn addition to Pd enhances the Pd-CO bond cleavage and improves TOF. The directly measured reactivity for $PdZn_a$ therefore confirms that $PdZn_{b1}$ structure is uniquely capable of CO_2 production in MSR, possibly because of stabilizing formate to high enough temperatures that it can be hydrolyzed by water. Further, the synthesis of $PdZn_a$ now allows direct comparison of the reactivity of Pd, $PdZn_a$, and $PdZn_{b1}$- summarized in Table 3.

Vacuum TPD CO and Methanol decomposition studies show that methoxide dehydrogenation to formaldehyde is most facile on Pd, and that this ease of dehydrogenation can help explain the lower activation energy for MSR on Pd when compared to PdZn. The addition of Zn to Pd then serves to weaken the Pd-CO binding energy, as shown in the CO TPD experiments, thus leading to the increase in TOF observed for PdZn when compared to Pd. The shift in overall product selectivity and reaction pathways between $PdZn_a$ and $PdZn_{b1}$ is explicable in terms of the energies of formation of the formaldehyde and CO products which arise from methanol decomposition. On Pd and $PdZn_a$ CO is made at lower energies than formaldehyde, while on $PdZn_{b1}$ formaldehyde is formed before CO. Thus in multiple turnover experiments methanol decomposes to formaldehyde on $PdZn_{b1}$, which can react with water or hydroxyls to make CO_2. On Pd and $PdZn_a$ decomposition to CO is more facile so that the formate hydro-oxidation pathway is bypassed.

In summary, this work presents the first study on the reactivity of $PdZn_a$, and demonstrates that $PdZn_a$ is not selective to CO_2 under MSR. Zn addition to Pd improves TOF, consistent with DFT predictions that Zn addition to Pd shifts the rate limiting step for MSR to formaldehyde decomposition. Methanol TPD experiments on Pd, $PdZn_a$, and $PdZn_{b1}$ materials allow for speculation that the $PdZn_{b1}$ phase stabilizes the formate produced from methanol dissociative adsorption to high enough temperatures that it can be hydrolyzed by water. The addition of water does not change the selectivity of the $PdZn_a$ towards CO_2, suggesting that the water is not activated by this phase. The ability to measure the explicit reactivity of this phase of PdZn has therefore allowed us to better understand the MSR reaction pathways on PdZn. Further, we can now understand the contribution of $PdZn_a$ to the several studies published for supported PdZn and where poor MSR selectivity to CO_2 has been attributed to both particle size effects and incom-

plete Pd alloying with Zn. Instead, it is possible that $PdZn_a$ which is much more active for MSR than Pd but similarly selective to CO is responsible for observed poor MSR selectivity. The observation of altered reaction pathways for Pd, PdZn alpha and beta phases also allows for speculation on the relation between crystal structure of the catalysts studied and their reactivity. The alpha and beta phases are structurally closely related in that the alpha phase is a solid solution with fcc structure while the beta-phase is fcc derived, but with a changed vertical dimension, making it tetragonal as illustrated in Figure 11. Thus we see that a relatively small change in crystallographic structure can drastically alter the catalytic activity both in terms of reaction pathways and energetics, suggesting that similarly fundamental and careful studies of catalytically relevant systems can lead to significant improvement in understanding of the structure--catalytic activity relationship of materials.

Acknowledgements

We gratefully acknowledge funding for this work provided by the U.S. Department of Energy for grant DE-FG02-05ER15712 and partial funding from grants DE-FG02-08ER46530 and DE-FG02-04ER15605. Also the National Science Foundation for Grant OISE 0730277, Partnerships for International Research and Education (PIRE). We also gratefully acknowledge computing resources provided by the New Mexico Computing Applications Center (NMCAC) on Encanto. Ambient Pressure XPS experiments were carried out at BESSY II, Helmholtz-Zentrum Berlin. A portion of the research was performed using EMSL, a national scientific user facility sponsored by the Department of Energy's Office of Biological and Environmental Research and located at Pacific Northwest National Laboratory. We thank Fernando Garzon of Los Alamos National laboratory for access to the micro-XRF.

References

[1] T.B. Massalski, Binary Alloy Phase Diagrams, Second ed., Materials Information Soc., Materials Park, Ohio, 1990.

[2] E.J. Peterson, B. Halevi, B. Kiefer, M.N. Spilde, A.K. Datye, J. Peterson, L. Daemen, A. Llobet, H. Nakotte, Aerosol synthesis and Rietveld analysis of tetragonal ([beta]1) PdZn, Journal of Alloys and Compounds, 509 (2011) 1463-1470.

[3] B. Halevi, E.J. Peterson, A. DeLaRiva, E. Jeroro, V.M. Lebarbier, Y. Wang, J.M. Vohs, B. Kiefer, E. Kunkes, M. Havecker, M. Behrens, R. Schlögl, A.K. Datye, Aerosol-Derived Bimetallic Alloy Powders: Bridging the Gap†, The Journal of Physical Chemistry C, 114 (2010) 17181-17190.

[4] N. Iwasa, S. Kudo, H. Takahashi, S. Masuda, N. Takezawa, Highly Selective Supported Pd Catalysts For Steam Reforming Of Methanol, Catalysis Letters, 19 (1993) 211-216.

[5] N. Iwasa, O. Yamamoto, T. Akazawa, S. Ohyama, N. Takezawa, Dehydrogenation Of Methanol To Methyl Formate Over Palladium Zinc-Oxide Catalysts, Journal of the Chemical Society-Chemical Communications, (1991) 1322-1323.

[6] N. Iwasa, S. Masuda, N. Ogawa, N. Takezawa, Steam Reforming of Methanol over Pd/Zno - Effect of the Formation of Pdzn Alloys Upon the Reaction, Applied Catalysis a-General, 125 (1995) 145-157.

[7] P. Bera, J.M. Vohs, Reaction of CH3OH on Pd/ZnO(0001) and PdZn/ZnO(0001) model catalysts, J. Phys. Chem. C, 111 (2007) 7049-7057.

[8] E. Jeroro, J.M. Vohs, Zn modification of the reactivity of Pd(111) toward methanol and formaldehyde, Journal of the American Chemical Society, 130 (2008) 10199-10207.

[9] W. Stadlmayr, S. Penner, B. Klotzer, N. Memmel, Growth, thermal stability and structure of ultrathin Zn-layers on Pd(111), Surface Science, 603 (2009) 251-255.

[10] C. Rameshan, W. Stadlmayr, C. Weilach, S. Penner, H. Lorenz, M. Havecker, R. Blume, T. Rocha, D. Teschner, A. Knop-Gericke, R. Schlogl, N. Memmel, D. Zemlyanov, G. Rupprechter, B. Klotzer, Subsurface-Controlled CO2 Selectivity of PdZn Near-Surface Alloys in H-2 Generation by Methanol Steam Reforming, Angewandte Chemie-International Edition, 49 (2010) 3224-3227.

[11] E.S. Ranganathan, S.K. Bej, L.T. Thompson, Methanol steam reforming over Pd/ZnO and Pd/CeO2 catalysts, Applied Catalysis A: General, 289 (2005) 153-162.

[12] T. Conant, A.M. Karim, V. Lebarbier, Y. Wang, F. Girgsdies, R. Schlogl, A. Datye, Stability of bimetallic Pd-Zn catalysts for the steam reforming of methanol, Journal of Catalysis, 257 (2008) 64-70.

[13] J.A. Rodriguez, Interactions in Bimetallic Bonding - Electronic and Chemical-Properties of Pdzn Surfaces, J. Phys. Chem., 98 (1994) 5758-5764.

[14] E. Jeroro, V. Lebarbier, A. Datye, Y. Wang, J.M. Vohs, Interaction of CO with surface PdZn alloys, Surface Science, 601 (2007) 5546-5554.

[15] A.C. Larson, R.B. VonDreele, General Structure Analysis System (GSAS), in, Los Alamos National Laboratory Report LAUR 86-748
2004.

[16] P.W. Stephens, Phenomenological model of anisotropic peak broadening in powder diffraction, Journal of Applied Crystallography, 32 (1999) 281-289.

[17] E.J. Peterson, B. Halevi, B. Kiefer, A.K. Datye, J. Peterson2, L. Daemon, a.H. Nakote, Aerosol synthesis and Rietveld analysis of tetragonal (b1) PdZn, Journal of Alloys and Compounds, (2010).

[18] G. Ertl, H. Knozinger, F. Schuth, J. Weitkamp, Handbook Of Hetergeneous Catalysis, in, Wiley-VCH Verlag GmbH & Co., Weinheim, 2008.

[19] W.K. Kuhn, J. Szanyi, D.W. Goodman, Co Adsorption on Pd(111) - the Effects of Temperature and Pressure, Surface Science, 274 (1992) L611-L618.

[20] P. Sautet, M.K. Rose, J.C. Dunphy, S. Behler, M. Salmeron, Adsorption and energetics of isolated CO molecules on Pd(111), Surface Science, 453 (2000) 25-31.

[21] G. Rupprechter, V.V. Kaichev, H. Unterhalt, A. Morkel, V.I. Bukhtiyarov, CO dissociation and CO hydrogenation on smooth and ion-bombarded Pd(111): SFG and XPS spectroscopy at mbar pressures, Appl. Surf. Sci., 235 (2004) 26-31.

[22] C.J. Powell, A. Jablonski, NIST Electron Effective-Attenuation-Length Databe, Version 1.3, 1.3 ed., National Institute of Standards and Technology, Gaithesburg, MD, 2011.

[23] G. Ketteler, D.F. Ogletree, H. Bluhm, H. Liu, E.L.D. Hebenstreit, M. Salmeron, In Situ Spectroscopic Study of the Oxidation and Reduction of Pd(111), Journal of the American Chemical Society, 127 (2005) 18269-18273.

[24] M. Salmeron, R. Schlogl, Ambient pressure photoelectron spectroscopy: A new tool for surface science and nanotechnology, Surface Science Reports, 63 (2008) 169-199.

[25] W. Stadlmayr, C. Rameshan, C. Weilach, H. Lorenz, M. Hävecker, R. Blume, T. Rocha, D. Teschner, A. Knop-Gericke, D. Zemlyanov, S. Penner, R. Schlögl, G. Rupprechter, B. Klötzer, N. Memmel, Temperature-Induced Modifications of PdZn Layers on Pd(111), The Journal of Physical Chemistry C, 114 (2010) 10850-10856.

[26] A.P. Tsai, S. Kameoka, Y. Ishii, PdZn=Cu: Can an intermetallic compound replace an element?, Journal of the Physical Society of Japan, 73 (2004) 3270-3273.

[27] A. Bayer, K. Flechtner, R. Denecke, H.P. Steinruck, K.M. Neyman, N. Rosch, Electronic properties of thin Zn layers on Pd(111) during growth and alloying, Surface Science, 600 (2006) 78-94.

[28] P. Bera, J.M. Vohs, Growth and structure of Pd films on ZnO(0001), The Journal of Chemical Physics, 125 (2006) 164713-164717.

[29] C.W. Zou, Y.Y. Wu, B. Sun, P.S. Xu, H.B. Pan, F.Q. Xu, Photoemission studies of initial oxidation for ultra-thin zinc film on 6H-SiC(0 0 0 1) surface with synchrotron radiation, Applied Surface Science, 253 (2007) 3761-3765.

[30] W.J. Pardee, G.D. Mahan, D.E. Eastman, R.A. Pollak, L. Ley, F.R. McFeely, S.P. Kowalczyk, D.A. Shirley, Analysis Of Surface-Plasmon And Bulk-Plasmon Contributions To X-Ray Photoemission Spectra, Physical Review B, 11 (1975) 3614-3616.

[31] J.Y. Lin, P. Jones, J. Guckert, E.I. Solomon, Variable Photon Energy Photoelectron Spectroscopic Study Of Co Adsorption To Coordinatively Unsaturated Tetrahedron Cu(I) And Zn(Ii) Sites On Cucl(111) And Zno(1010) Surfaces - D10 Contributions To Co Bonding And Activation, Journal of the American Chemical Society, 113 (1991) 8312-8326.

[32] C.W. Zou, Y.Y. Wu, B. Sun, W. Gao, P.S. Xu, Photoemission studies of Mn/ZnO(000-1) interface, Surface and Interface Analysis, 39 (2007) 865-870.

[33] S. Noothongkaew, R. Supruangnet, W. Meevasana, H. Nakajima, S. Limpijumnong, P. Songsiriritthigul, In situ monitoring of ZnO formation by photoemission spectroscopy, Applied Surface Science, 256 (2009) 980-983.

[34] W. Stadlmayr, C. Rameshan, C. Weilach, H. Lorenz, M. Havecker, R. Blume, T. Rocha, D. Teschner, A. Knop-Gericke, D. Zemlyanov, S. Penner, R. Schlogl, G. Rupprechter, B. Klotzer, N. Memmel, Temperature-Induced Modifications of PdZn Layers on Pd(111), J. Phys. Chem. C, 114 (2010) 10850-10856.

[35] Z.X. Chen, K.M. Neyman, K.H. Lim, N. Rosch, CH3O decomposition on PdZn(111), Pd(111), and Cu(111). A theoretical study, Langmuir, 20 (2004) 8068-8077.

[36] K.M. Neyman, K.H. Lim, Z.X. Chen, L.V. Moskaleva, A. Bayer, A. Reindl, D. Borgmann, R. Denecke, H.P. Steinruck, N. Rosch, Microscopic models of PdZn alloy catalysts: structure and reactivity in methanol decomposition, Physical Chemistry Chemical Physics, 9 (2007) 3470-3482.

[37] G.K. Smith, S. Lin, W.Z. Lai, A. Datye, D.Q. Xie, H. Guo, Initial steps in methanol steam reforming on PdZn and ZnO surfaces: Density functional theory studies, Surface Science, 605 (2011) 750-759.

[38] N.W. Cant, P.C. Hicks, B.S. Lennon, Steady-state oxidation of carbon monoxide over supported noble metals with particular reference to platinum, Journal of Catalysis, 54 (1978) 372-383.

[39] H.P. Koch, I. Bako, R. Schennach, Adsorption of small molecules on a (2 × 1) PdZn surface alloy on Pd(1 1 1), Surface Science, In Press, Corrected Proof.